The Knee 26 (2019) 2–13

Contents lists available at ScienceDirect

The Knee

Histopathological changes in the infrapatellar fat pad in an experimental rabbit model of early patellofemoral osteoarthritis

Binggang Wang [a], Yanfei Lang [b], Liu Zhang [a,b,*]

[a] Department of Orthopedic Surgery, Hebei Medical University, Shijiazhuang, China
[b] Department of Orthopedic Surgery, The Affiliated Hospital of North China University of Science and Technology, Tangshan, China

ARTICLE INFO

Article history:
Received 28 December 2017
Received in revised form 20 May 2018
Accepted 8 June 2018

Keywords:
Infrapatellar fat pad
Anterior knee pain
Patellofemoral osteoarthritis
Synovitis
Osteophyte
Knee

ABSTRACT

Background: The purpose of this study was to characterise the histopathological changes in the infrapatellar fat pad (IPFP) in the early stage of patellofemoral osteoarthritis (PFOA).

Methods: Sixty-four New Zealand white rabbits were randomly divided into experimental (n = 24), sham (n = 16), and control groups (n = 24). In the experimental group, denoted as the patellar ligament uneven shortening group (US group), the patellar ligament (PL) was folded eight millimetres and sutured. After eight weeks, all animals were euthanised, and magnetic resonance imaging (MRI) evaluation, wet IPFP weight measurement, and histopathological and immunohistochemistry analysis were performed to analyse the histopathological changes in the IPFPs.

Results: The maximum cross-sectional area (CSA) of the IPFPs in the sagittal position of MRI in the control group, sham group, and US group were $45.50 \pm 7.19\ mm^2$, $45.88 \pm 6.60\ mm^2$ (vs. control group, $P = 0.907$), and $53.83 \pm 8.24\ mm^2$ (vs. control group, $P = 0.015$; vs. sham group, $P = 0.035$), respectively. The MRI intensity of the IPFPs in the control group, sham group, and US group were 115.53 ± 28.85, 108.53 ± 26.73 (vs. control group, $P = 0.589$), and 154.52 ± 18.48 (vs. control group, $P = 0.002$; vs. sham group, $P = 0.002$), respectively. The wet weight of the IPFPs in the control group, sham group, and US group were 0.32 ± 0.05 g, 0.32 ± 0.04 g (vs. control group, $P = 0.895$), and 0.38 ± 0.06 g (vs. control group, $P = 0.017$; vs. sham group, $P = 0.033$), respectively. The Osteoarthritis Research Society International (OARSI) scores of the IPFPs in the US group were 6.00 ± 1.91, which was higher than the scores of 2.50 ± 2.02 ($P < 0.001$) in the control group and of 2.75 ± 1.67 ($P = 0.001$) in the sham group.

Conclusions: The histopathological changes of the IPFPs as determined via MRI and microscopic structure appeared to occur much earlier than cartilage damage in PFOA. Furthermore, detecting and treating the IPFP changes may offer aid in the diagnosis and treatment of PFOA.

1. Introduction

The infrapatellar fat pad (IPFP), also known as Hoffa's fat pad, is an intracapsular but extrasynovial structure located in the knee just under the patella and between the patellar tendon, femoral condyle, and tibial plateau. It is structurally similar to subcutaneous adipose tissue [1]. These fatty structures within the joints facilitate the distribution of synovial fluid and may absorb forces that are generated through the joint. The IPFP has long been believed to be mostly structural adipose tissue without any

* Corresponding author at: Department of Orthopedic Surgery, Hebei Medical University, Shijiazhuang, China and Department of Orthopedic Surgery, The Affiliated Hospital of North China University of Science and Technology, Tangshan, China.
E-mail address: zhliu130@sohu.com (L. Zhang).

https://doi.org/10.1016/j.knee.2018.06.010
0968-0160/

metabolic functions. However, recent studies suggest that besides the synovium, cartilage, and subchondral bone, the IPFP could play an important part in osteoarthritis (OA) and anterior knee pain [2]. The IPFP is highly vascularised and innervated, with its primary blood supply originating from the branches of the genicular arteries [3] and its sensory nerves originating from the posterior articular branch of the posterior tibial nerve [2]. The IPFP has been found to be affected by inflammation, hypertrophy, and fibrosis in generalised anterior knee pain or Hoffa's disease [2].

Patellofemoral osteoarthritis (PFOA) accounts for approximately 65% of patients with symptomatic knee OA, and PFOA is more likely than the tibiofemoral joint to be the source of knee OA symptoms. Moreover, even isolated mild radiographic PFOA can cause considerable symptoms that substantially impact daily living activities [4–6]. Little is known about PFOA, particularly the factors that contribute to its development, and most importantly, how to effectively manage this common and potentially debilitating condition [7].

Patellar maltracking is a translational or rotational deviation of the patella relative to any axis, such as subluxation or tilting [8]. Lateral subluxation is frequently accompanied by tilt. The combination of subluxation and tilting usually leads to OA due to abnormal loading of the articular cartilage [9]. Recent studies on PFOA have found that several factors may increase the risk of PFOA, including patella alta or baja, patella instability, patella dislocation, femoral trochlear dysplasia, limb malalignment, soft-tissue instability, and uneven muscle strength [10–16].

Based on this information, we created an uneven patellar ligament (PL) - shortening rabbit experimental model to mimic the early stage of PFOA. Little is known about IPFP changes in the early stage of PFOA, especially the histopathological changes. The aim of the current study was to characterise the histopathological changes of the IPFP in the early stage of PFOA.

2. Materials and methods

2.1. Animal handling

Animals were quarantined and acclimatised to the environmental conditions for one week before starting the experiment. The animal studies were reviewed and approved by the Ethics Committee for Experimental Animals of North China University of Science and Technology, and performed under the animal husbandry/management system in an appropriate environment with animal protection/welfare in mind.

2.2. Sample preparation

The subjects consisted of 24-week-old female New Zealand white rabbits ($n = 64$) (Vital River Experimental Animal Technical Co., Ltd., China) weighing approximately 2.64 ± 0.24 kg. They were randomly divided into an experimental group ($n = 24$), a sham group ($n = 16$) and a control group ($n = 24$). The intervention was performed on the left knee of the rabbits. After the administration of an intravenous injection of 30 mg/kg pentobarbital sodium to anaesthetise the rabbits, a vertical midline incision of approximately 2.5 cm in length was made on the left knee of the experimental group (US group) from the patella to the tibial tuberosity. Then, an approximately 2.5-cm medial parapatellar incision was made to open the capsule and expose the knee joint. The incision in the capsule was placed two centimetres medial to the medial margin of the patellar tendon without damaging the tendon. An eight-millimetre incision was made in the middle of patellar tendon just under the patella. Then, the medial patellar tendon was folded eight millimetres and sutured. The tendons were sutured using 4–0 tendon sutures and 3–0 absorbable sutures. Next, the capsule was opened and the skin was sutured using 3–0 absorbable sutures. The patella was not dislocated during the procedure (Figure 1). For the sham group, the same procedure was carried out except the medial patellar tendon was folded

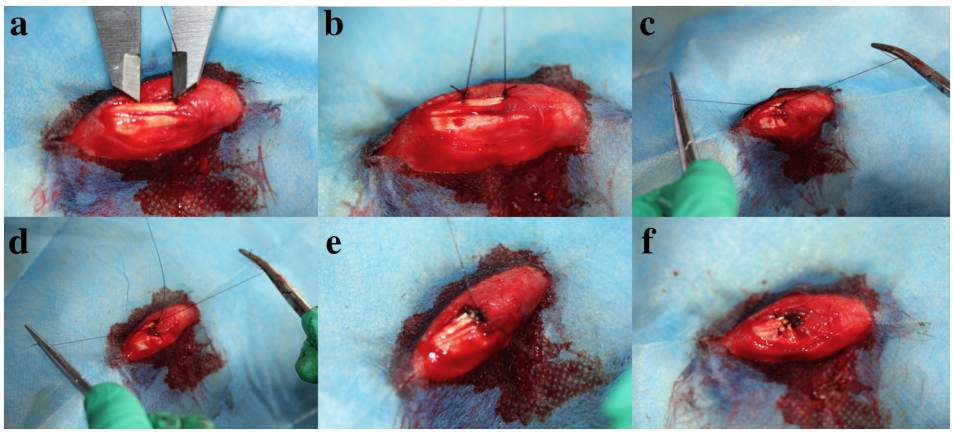

Figure 1. The animal modelling procedure. (a) An eight-millimetre incision was made in the middle of patellar tendon just under the patella measured by a vernier calipe. (b) Both ends of the medial ligament beside the incision were tied up by 3–0 absorbable sutures. (c) The ligament was shortened by traction of the two suture lines; (d) The tendon was sutured using 4–0 tendon sutures. (e) The traction line was tied together. (f) The ligament shortening was completed.

eight millimetres and sutured, and the tendon and capsule were sutured using 4–0 tendon sutures and 3–0 absorbable sutures. The right leg was not immobilised, and the rabbits lived in cages without the restriction of movement.

At eight weeks after surgery, all of the rabbits were euthanised by intravenous injection of a lethal dose of pentobarbital. The present study was conducted in accordance with the criteria established by the Ethics Committee for Experimental Animals of North China University of Science and Technology.

2.3. Magnetic resonance imaging evaluation

After euthanising the rabbits, the knees were removed as a single unit, and all structures ($n = 32$) were fixed in 10% neutral buffered formalin for one week. The knees were imaged in the sagittal plane on a 3.0-T whole-body magnetic resonance imaging unit (Magnetic Resonance System, GE Medical Systems, USA) using a cervical-thorax-lumbar 1:2 coil. The following sequence and parameters were used: a T1-weighted fat-suppressed three-dimensional (3D) gradient recall acquisition in the steady state; flip angle 150°; repetition time 695 ms; echo time 9.4 ms; field of view 260 mm; 320 × 75% matrix. The sagittal images were obtained at a partition thickness of 3.0 mm. The IPFPs were measured by manually drawing contours around the IPFP boundaries on the section-by-section T1-weighted sagittal MRIs using the software program GE Healthcare AW VolumeShareTM5. Computed single slices were reviewed to find the maximal cross-sectional area (CSA) (mm^2), which was selected to represent the IPFP size [1] (Figure 2). We measured the length of the PL on the MRI to analyse the change of PLs after modelling, and we measured the MRI intensity to analyse the IPFP change in the early stage of PFOA.

2.4. Wet weight of IPFPs

When the rabbits were euthanised, the knees were extracted as a unit, and the IPFPs of the US group ($n = 12$), the sham group ($n = 8$) and the control group ($n = 12$) were completely resected. We immediately measured the wet weight using an electronic scale (Mettler Instrumente AG, Type AE 240-S, Switzerland) and analysed the weight change of the IPFPs in the early stage of PFOA.

Figure 2. Drawing of disarticulation contours around the infrapatellar fat pad boundaries on section-by-section T1-weighted sagittal magnetic resonance images.

2.5. Gross observation and specimen processing

After disarticulation, the harvested knees of the US group (n = 12), the sham group (n = 8), and the control group (n = 12) were fixed in 10% neutral buffered formalin for MR imaging. Then, the femurs were cleaned, and their gross visual appearance was recorded with a digital camera (Canon 550D, Canon, Japan). The bony outgrowths in the medial margin were recorded according to Felson [18].

2.6. Tissue preparation and histopathological analysis

After MR scanning, the IPFPs were harvested for paraffin sections and then stained with haematoxylin–eosin. We calculated the mean cross-sectional area of adipose cells and calculated the number of adipose cells under each microscope (the morphology under 40× microscopy) using Image-Pro Plus (IPP) (Media Cybernetics, Inc., USA). Semi-quantitative histopathological analysis was established according to the Osteoarthritis Research Society International (OARSI) scoring system using four characteristics: synoviocytes, inflammatory infiltration, synovial stroma and cartilage/bone-detritus [19].

After MRI scanning, all of the femurs were decalcified with 15% ethylenediamine tetraacetic acid (EDTA)-Na^2 (pH 7.4), which was replaced once each week for 12 weeks. The distal ends of femurs were dehydrated with ethanol, embedded in paraffin, and cut into five-micrometre-thick sections (according to standard protocols). Two sections from each sample were stained with Toluidine Blue O. Then, two-colour digital images from each section were recorded under light microscopy (Olympus BX61, Olympus, Japan). Semi-quantitative histopathological analysis was performed by two experienced pathologists according to the OARSI scoring system using the following five characteristics: articular cartilage structure, proteoglycan content, cellularity, tidemark integrity, and osteophytes [19].

2.7. Immunohistochemistry for matrix metallopeptidase 9 and caspase-3

To further clarify the IPFP changes, the expressions of matrix metallopeptidase 9 (MMP-9) and caspase-3 in the IPFPs were detected by immunohistochemistry. Tissue sections were deparaffinised, rehydrated, and repaired in complex phosphoesterasum for 30 matrix metallopeptidase 9 min at 37 °C, and then incubated overnight at 4 °C with anti-rabbit MMP-9 (1:500) (Abcam Inc., England) and caspase-3 (1:500) (Abcam). Other procedures were performed according to instructions provided with the respective PV-6001 Polink-1 HRP DAB Detection System (ZSGB-BIO Corporation, China) and ZLI-9017 DAB kit (ZSGB-BIO Corporation, China). Sections were counterstained using Harris' haematoxylin solution (BASO Diagnostics Inc., China) for 30 s, and the target protein measurements in the IPFP tissue were evaluated by the average intensity of optical density. The average intensity of optical density, given as the integrated optical density per square millimetre (IOD/mm^2), was defined as the sum of the integrated option density in the region of interest (ROI) under a magnification of 10×. The ROI was defined as the adipose tissue under the synovium. These procedures were performed using Image-Pro Plus (Media Cybernetics, Inc., USA). The brown colour was developed using 3,3′-diaminobenzidine (DAB) (ZSGB-BIO Corporation, China). Areas that appeared yellow or brownish-yellow in colour were considered to be positively stained.

3. Statistical analysis

All data were analysed using Statistical Product and Service Solutions 20.0 (SPSS 20.0) software (SPSS, Chicago, IL, USA), and they are expressed as the mean ± standard deviation (SD). Statistical significance was defined as a *P*-value of <0.05. The data

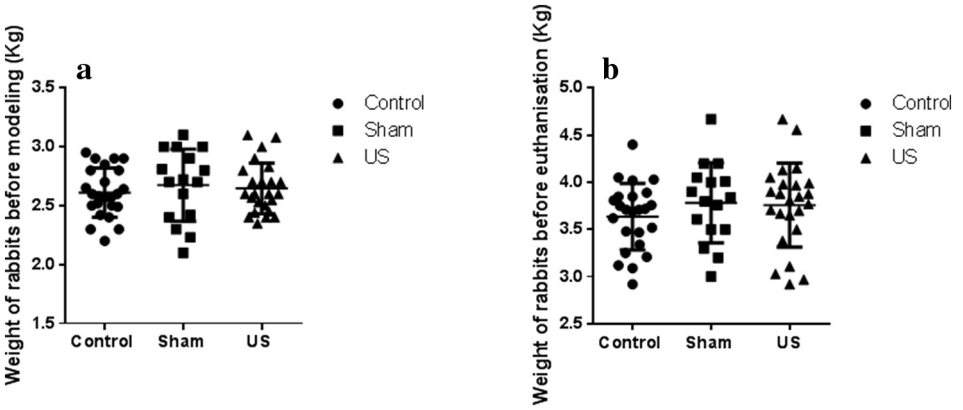

Figure 3. Weight of the rabbits of the three groups before modelling and before euthanisation. (a) Weight of the experimental rabbits before creating the model. (b) Weight of the experimental rabbits before they were euthanised. There were no significant differences in the body weights observed between the three groups ($P > 0.05$). US, experimental group.

were checked for a normal distribution using the Shapiro–Wilk test, and the data were normally distributed, except for the MRI intensity of the IPFPs and the IOD of MMP-9 and caspase-3 immunohistochemistry for the individual rabbits. Therefore, the normally distributed data were analysed by the independent sample *t*-test to compare the differences between the PLs in MRI, the CSA of the IPFPs, the wet weight of the IPFPs, the IPFP OARSI scores, the area of adipocytes in the IPFPs, and the number of adipocytes in the IPFPs. The MRI intensity of the IPFPs, the IOD of MMP-9 immunohistochemistry, and the IOD of caspase-3 immunohistochemistry for the individual rabbits were analysed by the Mann–Whitney *U* test to compare differences. Fisher's exact test was used to compare the number of osteophytes in the three groups.

4. Results

4.1. The rabbit weights

The rabbit weights of the control group, the sham group and the US group before modelling were 2.61 ± 0.21 kg, 2.67 ± 0.31 kg (vs. control group, $P = 0.437$), and 2.65 ± 0.21 kg (vs. control group, $P = 0.561$; vs. sham group, $P = 0.736$), respectively. The rabbit weights of the control group, the sham group and the US group before euthanising were 3.64 ± 0.35 kg, 3.78 ± 0.42 kg (vs. control group, $P = 0.238$), and 3.76 ± 0.45 kg (vs. control group, $P = 0.291$; vs. sham group, $P = 0.865$), respectively. No significant differences in body weights were observed between the three experimental groups during any observation period (Figure 3).

4.2. MRI evaluation

The length of the PLs in the control group, the sham group and the US group were 13.03 ± 1.06 mm, 13.52 ± 1.18 mm (vs. control group, $P = 0.348$), and 13.24 ± 1.41 mm (vs. control group, $P = 0.678$; vs. sham group, $P = 0.658$), respectively. The PLs in the three groups had no differences.

The maximum CSAs of the IPFPs in the sagittal position on MRI in the control group, the sham group and the US group were 45.50 ± 7.19 mm^2, 45.88 ± 6.60 mm^2 (vs. control group, $P = 0.907$), and 53.83 ± 8.24 mm^2 (vs. control group, $P = 0.015$; vs. sham group, $P = 0.035$), respectively. The maximum CSAs of the IPFPs in the US group were greater than those of the control and sham groups, indicating that the IPFP size in the US group was increased.

The MRI intensity of the IPFPs in the control group, the sham group and the US group were 115.53 ± 28.85, 108.53 ± 26.73 (vs. control group, $P = 0.589$), and 154.52 ± 18.48 (vs. control group, $P = 0.002$; vs. sham group, $P = 0.002$), respectively; the MRI intensity of the IPFP in the US group was increased significantly (Figure 4).

4.3. Wet weight of IPFPs

The IPFPs were completely resected when the rabbits were euthanised, and the wet weights were immediately obtained. The results of the control group, the sham group, and the US group were 0.32 ± 0.05 g, 0.32 ± 0.04 g (vs. control group, $P = 0.895$), and 0.38 ± 0.06 g (vs. control group, $P = 0.017$; vs. sham group, $P = 0.033$), respectively. The wet weight of the US group was significantly heavier compared with those of the control and sham groups (Figure 5).

4.4. Macroscopic evaluation

No significant differences were observed between the three groups with respect to the condyles of femurs, except for the osteophytes. The osteophytes appeared in the medial fringe of the condyles, one in the control group, one in the sham group (vs. control group, $P = 0.653$), and 11 in the US group (vs. control group, $P < 0.001$; vs. sham group, $P = 0.001$) (Figure 6).

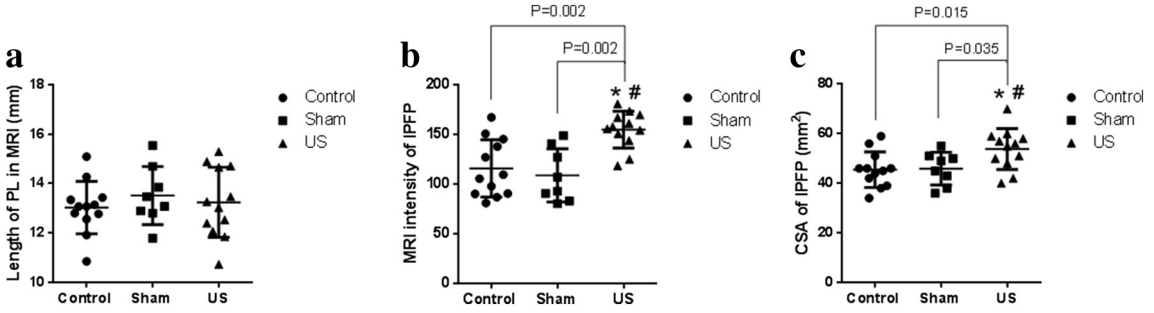

Figure 4. Measurement of parameters in magnetic resonance images (MRI). (a) Length of patellar ligaments (PLs) in the three-group analysis. (b) MRI intensity of the infrapatellar fat pads (IPFPs) in the control group, the sham group, and the experimental (US) group. (c) The maximum cross-sectional areas (CSAs) of the IPFPs in the control group, the sham group, and the US group. * vs. the control group and the US group, $P < 0.05$; # vs. the sham group and the US group, $P < 0.05$.

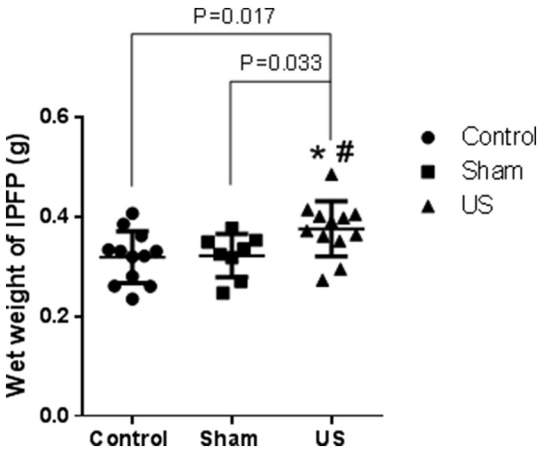

Figure 5. Wet weight of the infrapatellar fat pads (IPFPs). * vs. the control group and the experimental (US) group, $P < 0.05$; # vs. the sham group and the US group, $P < 0.05$.

4.5. Microscopic evaluation

With O staining, the osteophytes, which consist of chondrocytes and fibrocytes, appeared in the US group, and the chondrocytes of the osteophytes were growth disorders, i.e. overproliferation (Figure 7).

With haematoxylin and eosin staining, we observed that the IPFPs under the microscope consisted of a complex construction that was divided into six layers (Figure 8). Then, from the inner layer to the outer layer, the first layer was the synovium, which is made of simple synovial cells. The second layer included a large number of adipocytes, and there were no other tissues in this layer. The third layer was composed of blood vessels, and there were some collagen tissues around the vessels. The fourth layer was composed of a lobule collagen structure, which was full of adipocytes. The fifth layer was an interim layer between adipocytes and ligament, and it was composed of collagen and adipose tissue. The last layer was PL (Figure 9).

The normal synovium of the IPFP was smooth and flat, and it was composed of one layer of cells in the control group (Figure 10). The patellar maltracking caused the histopathological changes in the US group, and the synovial stroma villous hyperplasia

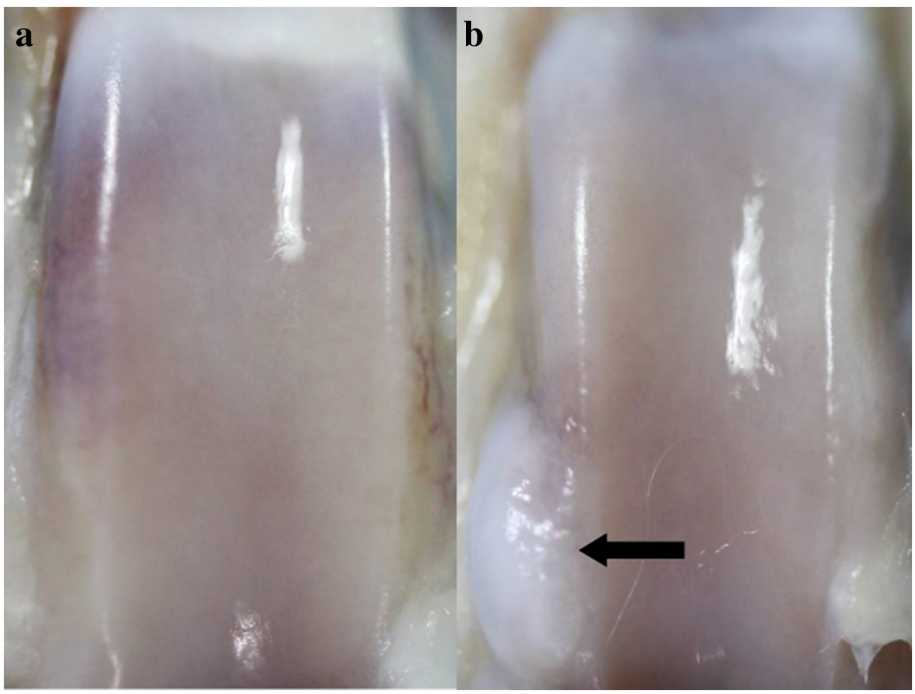

Figure 6. Macroscopic comparison of the femoral condylar. (a) The normal condylar from the control group. (b) The abnormal condylar with osteophyte in the medial margin as noted by the arrow from the experimental (US) group.

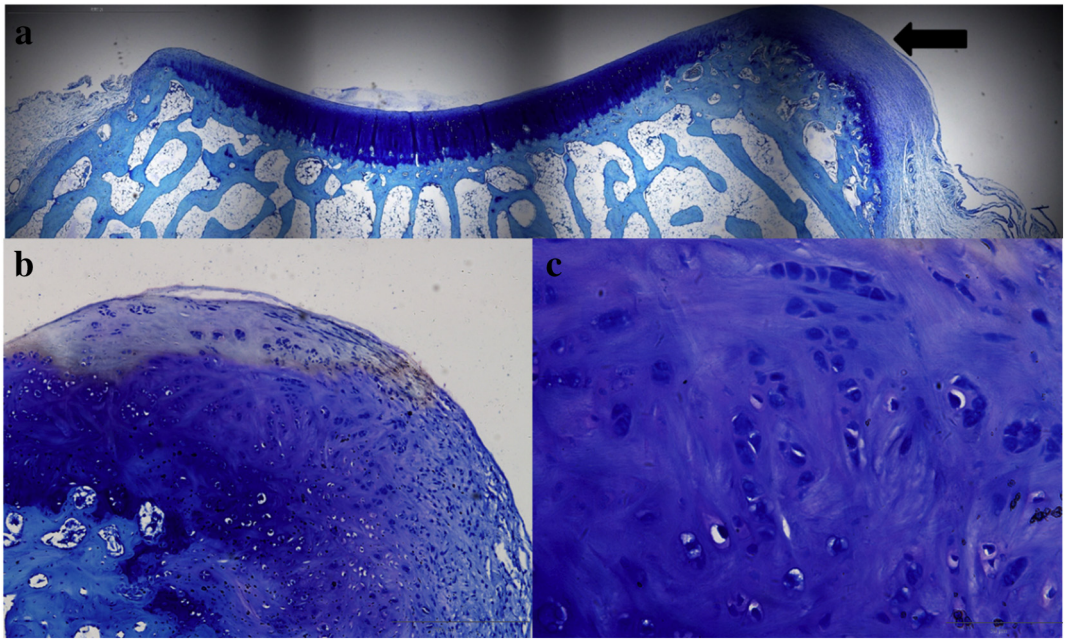

Figure 7. Histological morphology of femoral condylar with Toluidine Blue O stain from the experimental (US) group. (a) Overall condylar with osteophyte (morphology under 4× microscopy). (b) Histopathological changes of osteophyte (morphology under 10× microscopy). (c) Histopathological changes of osteophyte (morphology under 40× microscopy).

were more extensive than that in the control and sham groups (Figure 11); and the proliferation of fibroblasts was greater than that in the control and sham groups (Figure 11). Further, synovial stromal vascular hyperplasia was more extensive than that in the control and sham groups (Figure 11). Inflammatory infiltrate, which mainly involved lymphocytes in the IPFPs, was greater than that in the control and sham groups (Figure 11). Lymphocytes appeared alone or in colonies. Inflammatory infiltration in the ligaments mainly involved multinuclear giant cells, which appeared in colonies (Figure 11).

The CSAs of the adipose cells (the morphology under 40× microscopy) in the control group, the sham group and the US group were 419,417.69 ± 98,883.74 px, 406,573.81 ± 60,236.30 px (vs. control group, $P = 0.747$), and 411,884.83 ± 68,915.82 px (vs. control group, $P = 0.831$; vs. sham group, $P = 0.861$), respectively. There were no statistical differences among the groups. The number of adipose cells in the control group, the sham group, and the US group (the morphology under 40× microscopy) was 43.00 ± 6.37, 42.63 ± 6.23 (vs. control group, $P = 0.898$), and 50.33 ± 7.98 (vs. control group, $P = 0.021$; vs. sham group, $P = 0.034$), respectively. There was a statistical difference between the control group, the sham group and the US group, with the

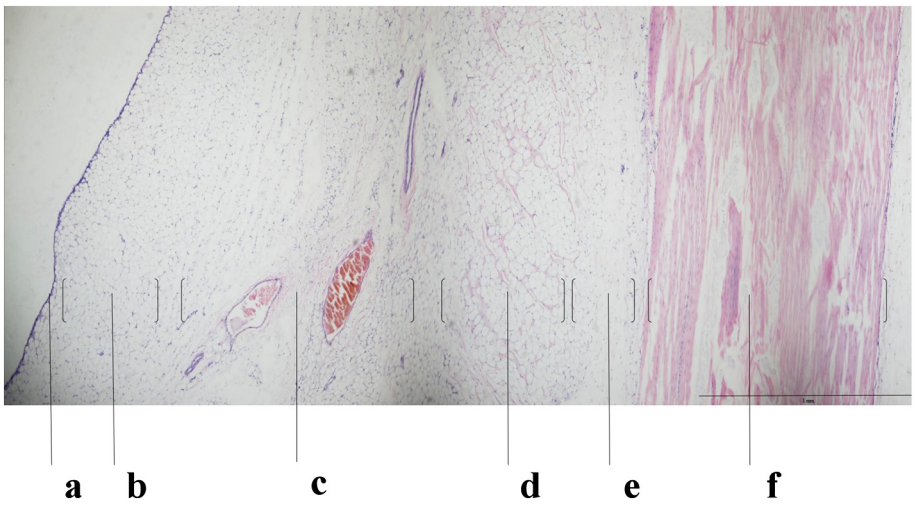

Figure 8. Entire layered structure of infrapatellar fat pad under microscopy (morphology under 4× microscopy). (a) Synovial layer. (b) Scatter adipose cell layer. (c) Blood vessel layer. (d) Septa interlobular adipose cell layer. (e) Junction of fat and ligament layer. (f) Patellar ligament layer.

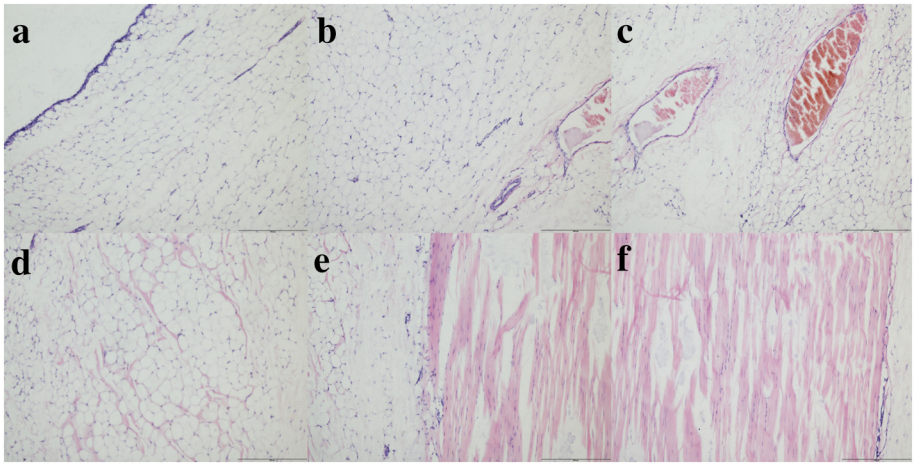

Figure 9. Layered structure of infrapatellar fat pad under microscopy (morphology under 10× microscopy). (a) Synovial layer. (b) Scatter adipose cell layer. (c) Blood vessel layer. (d) Septa interlobular adipose cell layer. (e) Junction of fat and ligament layer (f) Patellar ligament layer.

number of adipocytes being higher in the US group. According to the OARSI scores, the scores of the IPFPs in the US group were 6.00 ± 1.91, which was higher than the scores of 2.50 ± 2.02 ($P < 0.001$) in the control group and 2.75 ± 1.67 ($P = 0.001$) in the sham group; but there were no statistical differences between that in the control group and the sham group ($P = 0.776$) (Figure 12).

4.6. Immunohistochemistry evaluation

To further evaluate the IPFPs changes, the expressions of MMP-9 and caspase-3 in the IPFPs were detected by immunohistochemistry. The adipocytes' cytoplasms were positively stained. The expressions of MMP-9 and caspase-3 protein in the IPFPs were significantly higher than those in the control and the sham groups. The expressions of MMP-9 and caspase-3 protein in IPFPs were measured. The expression level of caspase-3 in the control group, the sham group, and the US group was 4.66 ± 3.49 IOD/mm^2, 4.31 ± 3.00 IOD/mm^2 (vs. control group, $P = 1.000$) and 18.03 ± 14.62 IOD/mm^2 (vs. control group, $P = 0.018$; vs. sham group, $P = 0.034$), respectively. The expression level of MMP-9 in the control group, the sham group, and the US group was 8.19 ± 6.99 IOD/mm^2, 8.19 ± 4.02 IOD/mm^2 (vs. control group, $P = 0.589$), and 20.05 ± 9.58 IOD/mm^2 (vs. control group, $P = 0.004$; vs. sham group, $P = 0.005$), respectively. The MMP-9 and caspase-3 expressions show that MMP-9 and caspase-3 in the IPFPs of the US group were more abundant than those in the normal IPFPs. An abundance of MMP-9 was positively correlated with cartilage damage, and an abundance of caspase-3 means that the rate of apoptosis was increasing (Figure 13).

5. Discussion

The objective of this study was to evaluate the IPFP changes in the early stage of PFOA to offer the new possible method for the early diagnosis and treatment of PFOA. We created the US animal model, which mimicked early-phase PFOA. There was no damage to cartilage except for osteophytes; the bony outgrowths are often found at joint margins and are typical radiographic findings of PFOA [18]. Osteophytes are the early manifestation of OA [19] and a typical radiographic finding during OA.

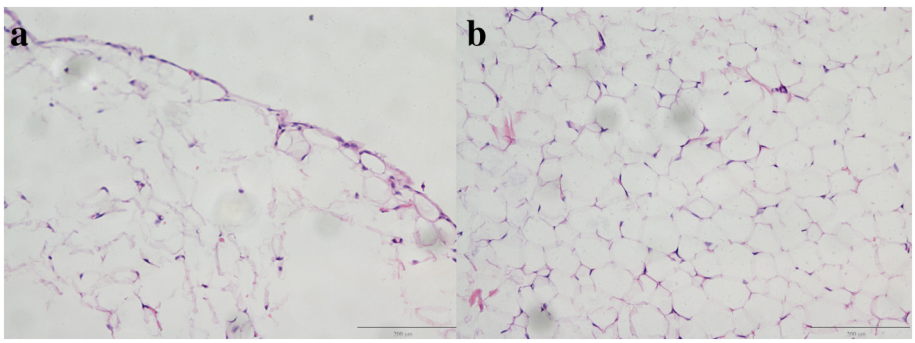

Figure 10. Normal infrapatellar fat pad. (a) Normal synovial membrane. (b) Normal adipose cell.

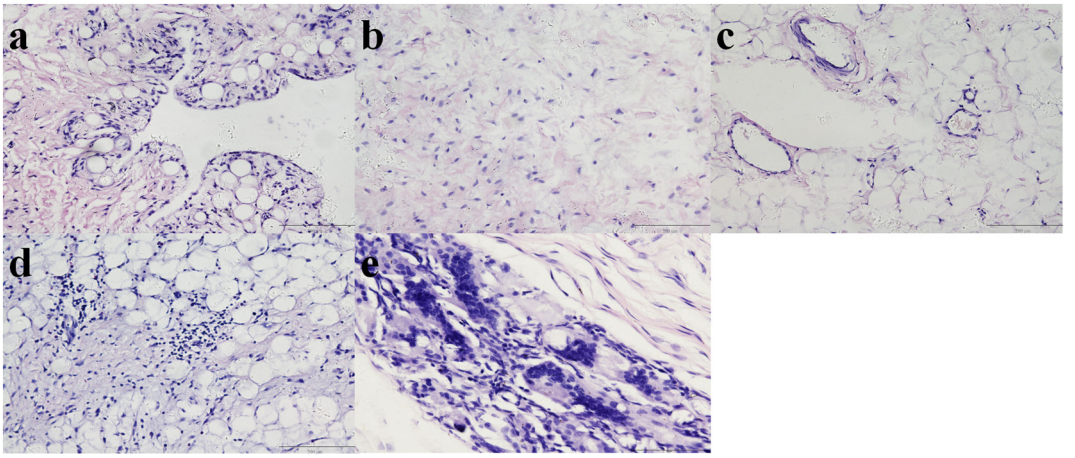

Figure 11. Histopathological infrapatellar fat pad changes. (a) Synovial stroma villous hyperplasia (morphology under 40× microscopy). (b) Proliferation of fibroblasts (morphology under 40× microscopy). (c) Synovial stromal vascular hyperplasia (morphology under 40× microscopy). (d) Inflammatory infiltration by lymphocytes (morphology under 40× microscopy). (e) Inflammatory infiltration by multinuclear giant cells (morphology under 40× microscopy).

Osteophytes are thought to form in response to joint instability [20]. This animal model did not change the actual length of PL; it only changed the patellar movement tracking, due to the medial instability and patellar tilt. There is no obvious cartilage damage in the early stage of PFOA, but the IPFP changes first. In this study, the IPFP was seen as a type of special synovium because it was enclosed by a large amount of synovium with adipose cells in the middle. Because the pathological changes of synovium are closely correlated with PFOA, we used the OARSI score of synovium to analyse the histopathological changes of IPFP to study the relationship of IPFPs with PFOA. The scores of IPFP in the US group were obviously higher than those in the two other groups, and there were statistical differences among them.

The histopathological IPFP structure changes in early PFOA are very evident [2]. Arthritis appears to accompany synovitis. In general, the degeneration of cartilage is mainly caused by the abrasion of articular cartilage due to mechanical stress or inflammatory and catabolic destruction accompanying synovitis [21, 22]. Synovitis can cause the inflammatory and catabolic destruction of the adjacent articular cartilage. When patellar tracking changes, the stress between the patella and femur changes and can lead to patellofemoral joint damage and limited range of motion [23, 24]. PL changes following total knee arthroplasty (TKA) and trauma have been reported mainly in clinical studies; however, minimal basic research of the IPFP in an animal model has previously been reported. PL changes in the rabbits in our experiment were similar to those described in clinical reports that imitated patellar maltracking caused by PL injury [25]. The results of the present study may contribute to a better understanding of the mechanism of IPFP histopathological changes in the early stage of PFOA caused by patellar maltracking in the clinical setting.

The MRI changes of PLs in the control group, the sham group, and the US group were not different. The changes in the US group noted on MRI showed that the IPFP was enlarged in early PFOA. The enlargement of the IPFP may be compensatory for the patellar maltracking, but this change may lead to pain in early PFOA. The IPFPs are space-occupying structures that promote joint lubrication and stability [26, 27]. The IPFP contains a framework of connective tissue septa interspersed among fat lobules [28, 29]. The IPFP is richly vascularised and innervated, and it plays a role in biomechanical support and neurovascular supply to adjacent structures. Substance P-immunoreactive nerve fibres have been found in the IPFP, indicating that it is a potential source of nociceptors that produce anterior knee pain [25, 29–31]. An IPFP disorder can be a source of anterior knee pain [32].

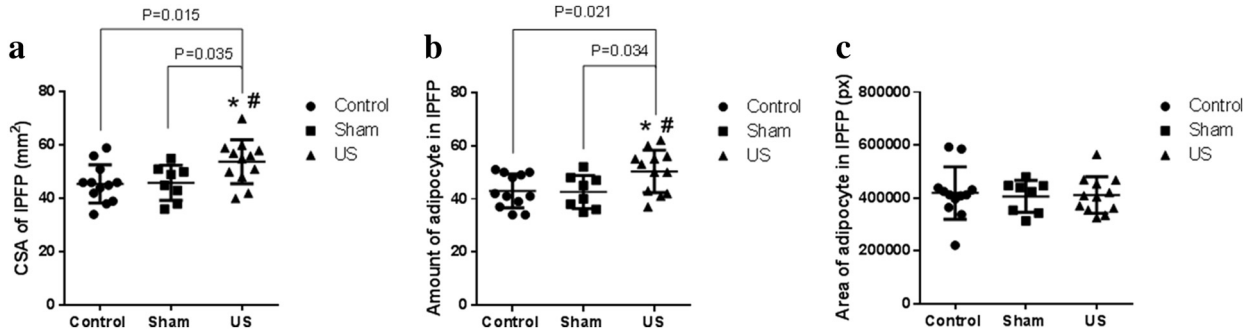

Figure 12. Histological analysis of the infrapatellar fat pads (IPFPs). (a) Osteoarthritis Research Society International (OARSI) scores of the IPFPs in the control group, the sham group, and the experimental (US) group. (b) Number of adipose cells of the IPFPs in the control group, the sham group, and the US group. (c) The cross-sectional area (CSA) of the adipose cells of the IPFPs in the control group, the sham group, and the US group. pixel. * vs. the control group and the US group, $P < 0.05$; # vs. the sham group and the US group, $P < 0.05$.

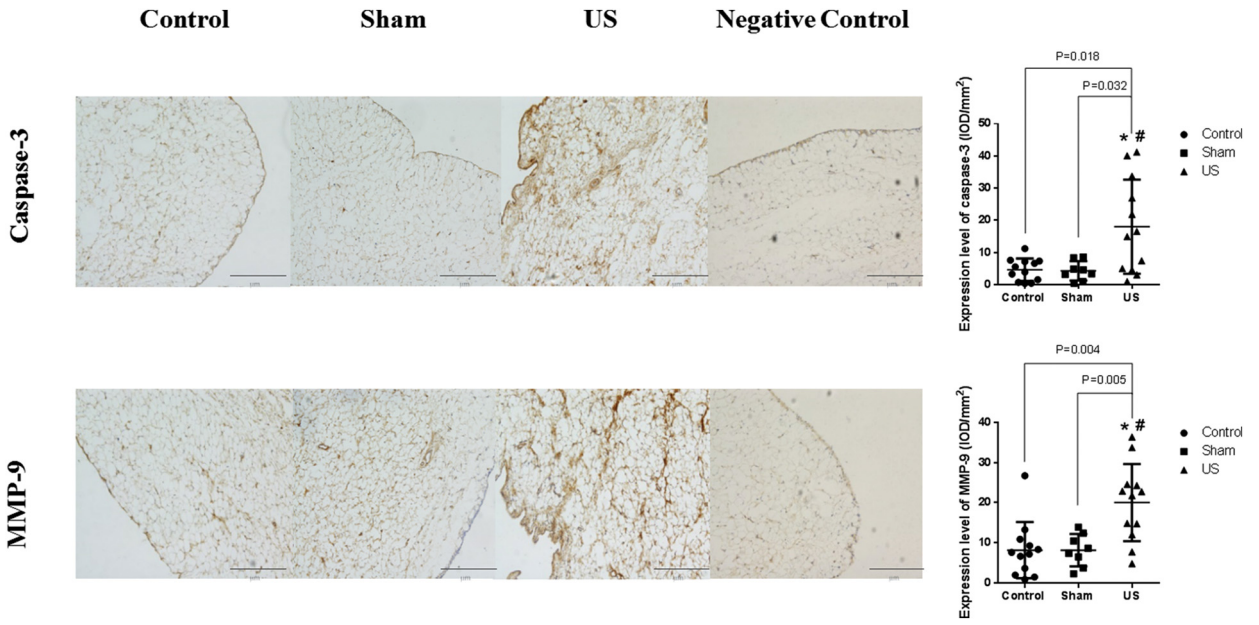

Figure 13. Immunohistochemical staining of the (infrapatellar fat pads) IPFPs, including caspase-3 and MMP-9 in the control group, the sham group, and the US groups (morphology under 10× microscopy). IOD, integrated optical density. * vs. the control group and the experimental (US) group, $P < 0.05$; # vs. the sham group and the US group, $P < 0.05$.

The MRI intensity of IPFP change indicates a change in the IPFP structure, which means the IPFP change occurs earlier than classic cartilage damage. Therefore, the change in IPFP on MRI may be an early sign of PFOA, which may offer a way to obtain an early diagnosis and treatment for PFOA.

The wet weight of the IPFPs was increased in the US group, which indicates hyperplasia of the IPFP in early PFOA, and it is in accordance with the CSA of the IPFP in MRI increasing in the early stage of PFOA. In our study, the IPFPs of the rabbits were complex layered constructions full of blood vessels, and not just adipocytes enclosed with synovium. The histopathological change of synovium in the IPFP is characterised by synovial lining hyperplasia, sublining fibrosis, and stromal vascularisation [33]. Inflammatory cell infiltration leads to the release of numerous inflammatory mediators, possibly acting to alter the sensitivity of sensory nerve afferent terminals, which can cause anterior knee pain [2]. In addition, subsequent fibrosis of the IPFP is likely to contribute to joint pain at the later stage of arthritis [2]. Furthermore, the number of adipocytes in the IPFP increased in the early stage of PFOA, but there were no enlarged adipocytes in the IPFP. The IPFP offers better buffering function by adipocyte proliferation; the increase in the number of blood vessels was an adaptation to this change. Synovitis is one of the key pathogenic factors for arthritis, and synovitis was present earlier than cartilage damage in our study. Furthermore, there is a very strong correlation that synovitis is associated with further worsening of the OA structure [34–40]. This indicates that synovitis is very important for arthritis, and it may be the first step for the development of arthritis.

In previous studies, some researchers have shown that there is a large number of leukocytes influxing from the vascular compartment in response to cytokines and cell adhesion molecules [41]. Other researchers have shown that macrophages and T-cell lymphocytes are the most predominant immune cells in OA synovium, whereas mast cells, B cells and plasma cells are also found, but to a lesser extent [42–44]. Debris from degraded hyaline cartilage released into the synovial cavity is likely to initiate synovial inflammation in OA. Synoviocytes react by producing additional pro-inflammatory mediators, which can attract immune cells, increase angiogenesis and induce a phenotypic shift in chondrocytes [45]. Therefore, a vicious cycle follows, as chondrocytes produce additional cytokines and proteolytic enzymes that eventually increase cartilage degradation and induce further synovial inflammation [46]. In this study, we observed lymphocytes in the IPFPs; they appeared independently or as a group in adipocytes, but the multinuclear giant cell appeared in the ligament.

In addition to the aforementioned findings, in this study we did not see the destruction of femoral and patellar cartilage, except for osteophytes, which have been considered to be an early manifestation of OA [19] in the US group. We also observed synovitis in the IPFPs of the US group, which appeared earlier than typical cartilage lesions in the early stage of OA.

There is evidence for synovitis being a common feature in OA. A series of recent papers from the OA Initiative also support the importance of synovitis prior to the radiographic manifestation of OA [47].

In our study, abnormal patellar tracking can also induce adipocyte cells in IPFP to apoptose, which was shown by the increased expression of caspase-3. Thus, these changes can contribute to fibroblast proliferation and vascular proliferation, which were similar to the increased MMP-9 expression in the IPFP. MMP-9 is the most complex member of the MMP family with its proteolytic activity against type-IV collagen and its upregulated expression in the serum and synovial joint fluid of patients with OA. The increased expression of MMP-9 has been positively correlated with cartilage damage [48].

The early detection of IPFP changes in FP OA may enable an earlier diagnosis and treatment of the condition. In addition, with this information about the IPFP changes, we may be able to delay the appearance of classical symptoms of PFOA.

6. Conclusions

Histopathological changes in the IPFP in the early stage of PFOA were synovial stroma villous hyperplasia, synovial stromal vascular hyperplasia, inflammatory infiltration, proliferation of fibroblasts and proliferation of adipocytes, which may contribute to the anterior knee pain and worsen the PF cartilage. The histopathological changes of the IPFPs as determined via MRI and microscopic structure appeared to occur much earlier than cartilage damage in PFOA. Furthermore, detecting and treating the IPFP changes may offer aid in the diagnosis and treatment of PFOA, but the IPFP histopathological changes in the later stage of PFOA need to be further explored.

Conflicts of interest

The authors declare that they have no competing interests.

Author contributions

B.G.W. and L.Z. conceptualised and designed the study. B.G.W. and Y.F.L. performed the anaesthesia procedures and the animal model making. B.G.W. and Y.F.L. performed animal feeding, histological and immunohistochemical analyses, scoring systems and image analyses, and histomorphometric analyses. All authors read and approved the final manuscript for publication.

Acknowledgements

The authors would like to thank Shuang Li and Liru Dong for IPFP specimen making and analysis; the authors would like to thank Muwei Dai, Guangyuan Liu and Yu Gou for providing technical and assessment support during immunohistochemical analysis. The study was supported by the National Natural Science Foundation of China (NSFC 31171136), the Major Project of Nature Science Foundation of Hebei Province (H2016209176) and the Scientific Innovation Team Foundation of Tangshan City (No. 15130208C). All experiments were approved by the Ethics Committee for Experimental Animals of North China University of Science and Technology.

Appendix A. Supplementary data

Supplementary data to this article can be found online at https://doi.org/10.1016/j.knee.2018.06.010.

References

[1] Teichtahl AJ, Wulidasari E, Brandy SR, Wang Y, Wluka AE, Ding C, et al. A large infrapatellar fat pad protects against knee pain and lateral tibial cartilage volume loss. Arthritis Res Ther 2015;10(17):318.
[2] Clements KM, Ball AD, Jones HB, Brinckmanns S, Read SJ, Murray F. Cellular and histopathological changes in the infrapatellar fat pad in the monoiodoacetate model of osteoarthritis pain. Osteoarthritis Cartilage 2009;17(6):805–12.
[3] Nemschak G, Pretterklieber ML. The patellar arterial supply via the infrapatellar fat pad (of Hoffa): a combined anatomical and angiographical analysis. Anat Res Int 2012;2012(4–5):713838.
[4] Duncan R, Hay E, Saklatvala J, Croft P. Prevalence of radiographic osteoarthritis: it all depends on your point of view. Rheumatology 2006;45(6):757–60.
[5] Duncan R, Peat G, Thomas E, Wood L, Hay E, Croft P. How do pain and function vary with compartmental distribution and severity of radiographic knee osteoarthritis? Rheumatology 2008;47(11):1704–7.
[6] Duncan R, Peat G, Thomas E, Wood L, Hay E, Croft P. Does isolated patellofemoral osteoarthritis matter? Osteoarthritis Cartilage 2009;17(9):1151–5.
[7] Crossley KM, Hinman RS. The patellofemoral joint: the forgotten joint in knee osteoarthritis. Osteoarthritis Cartilage 2011;19(7):765–7.
[8] Sakai N, Luo ZP, Rand JA, An KN. The influence of weakness in the vastus medialis oblique muscle on the patellofemoral joint: an in vitro biomechanical study. Clin Biomech 2000;15(5):335–9.
[9] Souza DR, Gross MT. Comparison of vastus medialis obliquus: vastus lateralis muscle integrated electromyographic ratios between healthy subjects and patients with patellofemoral pain. Phys Ther 1991;71(4):310–6.
[10] Tang SF, Chen CK, Hsu R, Chou SW, Hong WH, Lew HL. Vastus medialis obliquus and vastus lateralis activity in open and closed kinetic chain exercises in patients with patellofemoral pain syndrome: an electromyographic study. Arch Phys Med Rehabil 2001;82(10):1441–5.
[11] Koëter S, Diks MJF, Anderson PG, Wymenga AB. A modified tibial tubercle osteotomy for patellar maltracking. J Bone Joint Surg Br 2007;89(2):180–5.
[12] Wu SH, Chu NK, Liu YC, Chen CK, Tang SF, Cheng CK. Relationship between the EMG ratio of muscle activation and bony structure in osteoarthritic knee patients with and without patellar malalignment. J Rehabil Med 2008;40(5):381–6.
[13] Bollier M, Ikerson JP. The role of trochlear dysplasia in patellofemoral instability. J Am Acad Orthop Surg 2011;19(1):8–16.
[14] Lin F, Wilson NA, Makhsous M, Press JM, Koh JL, Nuber GW, et al. In vivo patellar tracking induced by individual quadriceps components in individuals with patellofemoral pain. J Biomech 2010;43(2):235–41.
[15] Tan SHS, Ibrahim MM, Lee ZJ, Chee YKM, Hui JH. Patellar tracking should be taken into account when measuring radiographic parameters for recurrent patellar instability. Knee Surg Sports Traumatol Arthrosc 2017. https://doi.org/10.1007/s00167-017-4795-0.
[16] Stefanik JJ, Zhu Y, Zumwalt AC, Gross KD, Clancy M, Lynch JA, et al. Association between patella alta and the prevalence and worsening of structural features of patellofemoral joint osteoarthritis: the multicenter osteoarthritis study. Arthritis Care Res (Hoboken) 2010;62(9):1258–65.
[18] Felson DT, Gale DR, Elon Gale M, Niu J, Hunter DJ, Goggins J, et al. Osteophytes and progression of knee osteoarthritis. Rheumatology (Oxford) 2005;44(1):100–4.
[19] Laverty S, Girard CA, Williams JM, Hunziker EB, Pritzker KP. The OARSI histopathology initiative-recommendations for histological assessments of osteoarthritis in the rabbit. Osteoarthritis Cartilage 2010;18(3):53–65.

[20] Hsia AW, Anderson MJ, Heffner MA, Lagmay EP, Zavodovskaya R, Christiansen BA. Osteophyte formation after ACL rupture in mice is associated with joint restabilization and loss of range of motion. J Orthop Res 2016;35(3):466–73.
[21] Abe H, Rodgers KE, Ellefson D, diZerega GS. Kinetics of interleuken-1 and tumor necrosis factor secretion by rabbit macrophages recovered from the peritoneal cavity after surgery. J Invest Surg 1991;4(2):141–51.
[22] Radin EL, Burr DB, Caterson D, Fyhrie D, Brown TD, Boyd RD. Mechanical determinants of osteoarthrosis. Semin Arthritis Rheum 1991;21(3 suppl. 2):12–21.
[23] Järvelä T, Paakkala T, Kannus P, Järvinen M. The incidence of patellofemoral osteoarthritis and associated findings 7 years after anterior cruciate ligament reconstruction with a bone-patellar tendon-bone autograft. Am J Sports Med 2001;29(1):18–24.
[24] Singerman R, Davy DT, Goldberg VM. Effects of patella alta and patella infera on patellofemoral contact forces. J Biomech 1994;27(8):1059–65.
[25] Liu YP, Li SZ, Yuan F, Xia J, Yu X, Liu X, et al. Infrapatellar fat pad may be with tendon repairing ability and closely related with the developing process of patella baja. Med Hypotheses 2011;77(4):620–3.
[26] Davies DV, White JE. The structure and weight of synovial fat pads. J Anat 1961;95:30–7.
[27] Gallagher J, Tierney P, Murray P, O'Brien M. The infrapatellar fat pad: anatomy and clinical correlations. Knee Surg Sports Traumatol Arthrosc 2005;13(4):268–72.
[28] Saddik D, McNally EG, Richardson M. MRI of Hoffa's fat pad. Skeletal Radiol 2004;33(8):433–44.
[29] Wagrowska-Danielewicz M. Distribution of substance P nerve fibers in the knee joint in patients with anterior knee pain syndrome: a preliminary report. Knee Surg Sports Traumatol Arthrosc 1999;7(3):177–83.
[30] Dye SF. The pathophysiology of patellofemoral pain: a tissue homeostasis perspective. Clin Orthop Relat Res 2005;436:100–10.
[31] Wojtys EM, Beaman DN, Glover RA, Janda D. Innervation of the human knee joint by substance-P fibers. Arthroscopy 1990;6(4):254–63.
[32] Tsavalas N, Karantanas AH. Suprapatellar fat-pad mass effect: MRI findings and correlation with anterior knee pain. AJR Am J Roentgenol 2013;200(3):W291–6.
[33] Prieto-Potin I, Largo R, Roman-Blas JA, Herrero-Beaumont G, Walsh DA. Characterization of multinucleated giant cells in synovium and subchondral bone in knee osteoarthritis and rheumatoid arthritis. BMC Musculoskelet Disord 2015;16:226.
[34] Mathiessen A, Slatkowsky-Christensen B, Kvien TK, Hammer HB, Haugen IK. Ultrasound-detected inflammation predicts radiographic progression in hand osteoarthritis after 5 years. Ann Rheum Dis 2016;75(5):825–30.
[35] de Lange-Brokaar BJ, Ioan-Facsinay A, Yusuf E, Kroon HM, Zuurmond AM, Stojanovic-Susulic V, et al. Evolution of synovitis in osteoarthritic knees and its association with clinical features. Osteoarthritis Cartilage 2016;24(11):1867–74.
[36] Conaghan PG, D'Agostino MA, Le Bars M, Baron G, Schmidely N, Wakefield R, et al. Clinical and ultrasonographic predictors of joint replacement for knee osteoarthritis: results from a large, 3-year, prospective EULAR study. Ann Rheum Dis 2010;69(4):644–7.
[37] Collins JE, Losina E, Nevitt MC, Roemer FW, Guermazi A, Lynch JA, et al. Semiquantitative imaging biomarkers of knee osteoarthritis progression: data from the FNIH OA Biomarkers Consortium. Arthritis Rheumatol 2016;68(10):2422–31.
[38] Kortekaas MC, Kwok WY, Reijnierse M, Kloppenburg M. Inflammatory ultrasound features show independent associations with progression of structural damage after over 2 years of follow-up in patients with hand osteoarthritis. Ann Rheum Dis 2015;74(9):1720–4.
[39] Haugen IK, Slatkowsky-Christensen B, Boyesen P, Sesseng S, van der Heijde D, Kvien TK. MRI findings predict radiographic progression and development of erosions in hand osteoarthritis. Ann Rheum Dis 2016;75(1):117–23.
[40] Damman W, Liu R, Bloem JL, Rosendaal FR, Reijnierse M, Kloppenburg M. Bone marrow lesions and synovitis on MRI associate with radiographic progression after 2 years in hand osteoarthritis. Ann Rheum Dis 2017;76(1):214–7.
[41] Scanzello CR, Goldring SR. The role of synovitis in osteoarthritis pathogenesis. Bone 2012;51(2):249–57.
[42] Klein-Wieringa IR, de Lange-Brokaar BJ, Yusuf E, Andersen SN, Kwekkeboom JC, Kroon HM, et al. Inflammatory cells in patients with end stage knee osteoarthritis: a comparison between the synovium and the infrapatellar fat pad. J Rheumatol 2016;43(4):771–8.
[43] Deligne C, Casulli S, Pigenet A, Bougault C, Campillo-Gimenez L, Nourissat G, et al. Differential expression of interleukin-17 and interleukin-22 in inflamed and non-inflamed synovium from osteoarthritis patients. Osteoarthritis Cartilage 2015;23(11):1843–52.
[44] de Lange-Brokaar BJ, Ioan-Facsinay A, van Osch GJ, Zuurmond AM, Schoones J, Toes RE, et al. Synovial inflammation, immune cells and their cytokines in osteoarthritis: a review. Osteoarthritis Cartilage 2012;20(12):1484–99.
[45] Goldring MB. Chondrogenesis, chondrocyte differentiation, and articular cartilage metabolism in health and osteoarthritis. Ther Adv Musculoskelet Dis 2012;4:269–85.
[46] Berenbaum F. Osteoarthritis as an inflammatory disease (osteoarthritis is not osteoarthrosis!). Osteoarthritis Cartilage 2013;21(1):16–21.
[47] Mathiessen A, Conaghan PG. Synovitis in osteoarthritis: current understanding with therapeutic implications. Arthritis Res Ther 2017;19(1):18.
[48] Zeng GQ, Chen AB, Li W, Song JH, Gao CY. High MMP-1, MMP-2, and MMP-9 protein levels in osteoarthritis. Genet Mol Res 2015;14(4):14811–22.